Broadly neutralizing anti-HIV-1 antibodies disrupt a hinge-related function of gp41 at the membrane interface

Likai Song[a,b,1], Zhen-Yu J. Sun[c,1], Kate E. Coleman[a], Michael B. Zwick[d], Johannes S. Gach[d], Jia-huai Wang[c,e,f], Ellis L. Reinherz[a,b,e,2], Gerhard Wagner[c], and Mikyung Kim[b,e,2]

[a]Cancer Vaccine Center and [e]Laboratory of Immunobiology and Department of Medical Oncology, Dana–Farber Cancer Institute, Boston, MA 02115; Departments of [b]Medicine, [c]Biological Chemistry and Molecular Pharmacology, and [f]Pediatrics Harvard Medical School, Boston, MA 02115; and [d]Department of Immunology and Microbial Science, The Scripps Research Institute, La Jolla, CA 92037

Edited by Robert C. Gallo, University of Maryland, Baltimore, MD, and approved April 6, 2009 (received for review February 10, 2009)

A vaccine capable of stimulating protective antiviral antibody responses is needed to curtail the global AIDS epidemic caused by HIV-1. Although rarely elicited during the course of natural infection or upon conventional vaccination, the membrane-proximal ectodomain region (MPER) of the HIV-1 glycoprotein of M_r 41,000 (gp41) envelope protein subunit is the target of 3 such human broadly neutralizing antibodies (BNAbs): 4E10, 2F5, and Z13e1. How these BNAbs bind to their lipid-embedded epitopes and mediate antiviral activity is unclear, but such information might offer important insight into a worldwide health imperative. Here, EPR and NMR techniques were used to define the manner in which these BNAbs differentially recognize viral membrane-encrypted residues configured within the L-shaped helix–hinge–helix MPER segment. Two distinct modes of antibody-mediated interference of viral infection were identified. 2F5, like 4E10, induces large conformational changes in the MPER relative to the membrane. However, although 4E10 straddles the hinge and extracts residues W672 and F673, 2F5 lifts up residues N-terminal to the hinge region, exposing L669 and W670. In contrast, Z13e1 effects little change in membrane orientation or conformation, but rather immobilizes the MPER hinge through extensive rigidifying surface contacts. Thus, BNAbs disrupt HIV-1 MPER fusogenic functions critical for virus entry into human CD4 T cells and macrophages either by preventing hinge motion or by perturbing MPER orientation. HIV-1 MPER features important for targeted vaccine design have been revealed, the implications of which extend to BNAb targets on other viral fusion proteins.

membrane-proximal ectodomain region | neutralizing antibody | vaccine design | AIDS | fusion

The 120-nm-diameter HIV-1 is a retrovirus that has a small genome consisting of 9 genes. The enveloped virion surface expresses the trimeric glycoprotein of M_r 160,000 (gp160) spike protein, whose gp120 and gp41 subunits are assembled into noncovalently associated heterodimers. Unlike gp120, each gp41 subunit has a transmembrane segment (TM) that inserts into the membrane of the virus. The membrane proximal ectodomain region (MPER) links this TM to the folded gp41 ectodomain. Entry of HIV-1 into human T cells is mediated by attachment of the gp120 subunit to receptor CD4 and then binding to the coreceptor (CCR5 or CXCR4) (1). These interactions result in structural rearrangement of the gp41 subunit, followed by fusion of viral and host cell membranes (2, 3). Thus, antibody-mediated protection against HIV-1 must target the gp120/gp41 envelope trimer, the only viral protein exposed on the virion surface.

Although high-titer, strain-specific neutralizing antibodies are readily generated during the course of natural infection or against subunit vaccines, broadly neutralizing antibodies (BNAbs), in contrast, are rarely produced (reviewed in ref. 4). Sequence variability, extensive glycosylation, and immunodominance of those exposed, largely variable segments subvert immune responsiveness (5, 6). Hence, only 5 BNAbs have been isolated to date from human patient-derived material (7–14). Among them, 3 (2F5, 4E10, and Z13e1) bind to the MPER of gp41, a region known to be important for viral fusion (Fig. 1*A*) (15, 16). In a recent structural study, it was shown that the MPER adopts a metastable L-shaped structure embedded in the viral membrane comprising a N-terminal helical segment (residues 664–672) tilted with respect to the membrane, and a near-flat C-terminal helix (675–683) connected via a flexible hinge (Fig. 1*B*) (17). This membrane-embedded feature makes the segment less accessible to immune attack and harbors strategically positioned tryptophan residues associated with viral fusion. Further structural analysis of 4E10 bound to the HxB2 MPER from clade B strain suggests that the neutralization mechanism of 4E10 is correlated with the ability of the antibody to extract core epitope residues W672 and F673 buried in the lipid acyl chains. In the present study, we examine and compare the molecular mechanisms of viral neutralization mediated by the 2 other BNAbs with that of 4E10, whose binding sites are adjacent or overlapping such that they sterically crossblock one another. Our studies reveal how distinct mechanisms of viral inhibition can be targeted on this one discrete envelope segment.

Results

Immersion Depth Changes of MPER Residues upon 2F5 and Z13e1 Binding by EPR. EPR and NMR analyses were performed with 2F5 and Z13e1 by using an HxB2 MPER (N674D) variant to preserve the optimal core epitope recognition of Z13e1 (11). We note also that D674 is the consensus residue for group M HIV-1. Results of the NMR study suggest that although there are perturbations to the local environment surrounding residue D674, the variant has little conformational change compared with the N674 sequence (Figs. S1 and S2). Membrane immersion depths of the spin-labeled side chains (R1) using site-directed mutant MPER peptides were determined by the ratio of the collision accessibility values of relaxant reagents, oxygen, and nickel(II) ethylenediaminediacetic acid (NiEDDA), measured via power saturation techniques (18) (Fig. 1 *C* and *D*). Both the sequential immersion depth values and the periodicity of accessibility parameters (Fig. S3) suggest that the variant MPER segment retains the same membrane orientation and L-shaped configuration as the wild-type MPER.

Author contributions: L.S., Z.-Y.J.S., E.L.R., G.W., and M.K. designed research; L.S., Z.-Y.J.S., K.E.C., and M.K. performed research; L.S., Z.-Y.J.S., M.B.Z., J.S.G., G.W., and M.K. contributed new reagents/analytic tools; L.S., Z.-Y.J.S., J.-h.W., E.L.R., G.W., and M.K. analyzed data; and L.S., Z.-Y.J.S., E.L.R., and M.K. wrote the paper.

The authors declare no conflict of interest.

This article is a PNAS Direct Submission.

[1]L.S. and Z.-Y.J.S. contributed equally to this work.

[2]To whom correspondence may be addressed. E-mail: ellis_reinherz@dfci.harvard.edu or mikyung_kim@dfci.harvard.edu.

This article contains supporting information online at www.pnas.org/cgi/content/full/0901474106/DCSupplemental.

MICROBIOLOGY

Downloaded at Palestinian Territory, occupied on December 19, 2021

www.manaraa.com

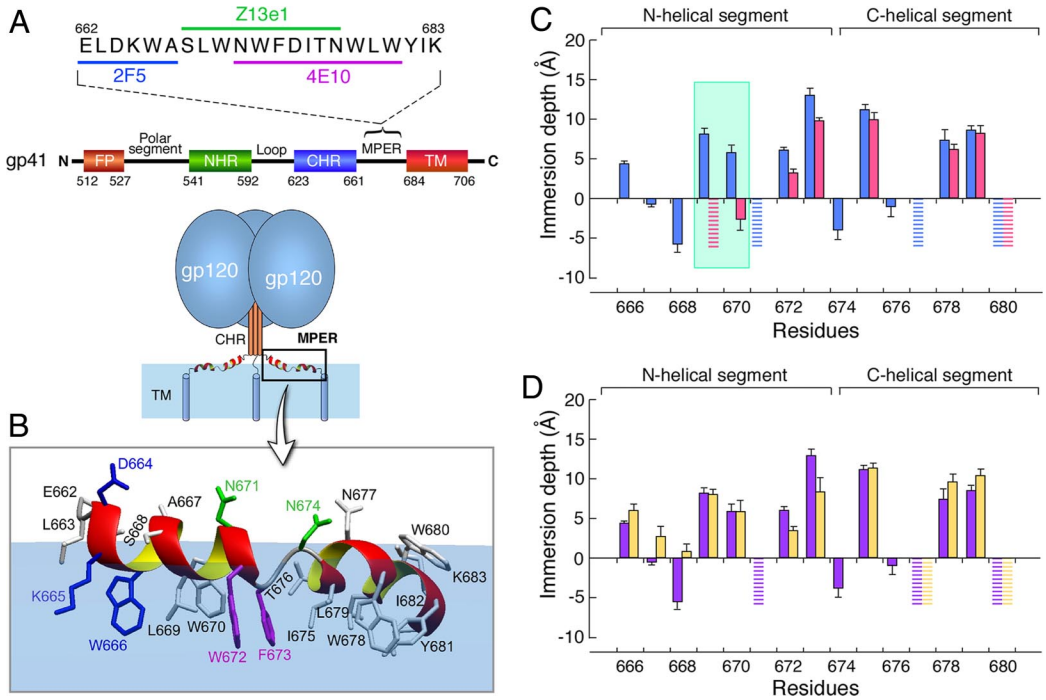

Fig. 1. The structure of the MPER and immersion depth changes induced by 2F5 and Z13e1. (*A*) Schematic diagram of HIV-1 gp41. FP, fusion peptide region; NHR and CHR, N- and C-terminal α-helices of heptad repeat, respectively; and TM, transmembrane domain. The minimal peptide epitopes of BNAbs are indicated for 2F5 (blue), Z13e1 (green), and 4E10 (magenta). (*B*) A simple model of env including MPER and TM based on one of the 3-dimensional structural features of HIV-1/SIV-1 trimeric env (37–40) and the NMR structure of the HxB2 MPER in a virion mimic membrane (dioleoyl phosphatidylcholine/sphingomyelin/dioleoyl phosphatidylethanolamine/dioleoyl phosphatidylglycerol/cholesterol) surface (blue plane). Residues essential for antibody neutralization are color coded with blue for 2F5, green for Z13e1, and magenta for 4E10. Note that N674 rather than D674 is shown. (*C*) Immersion depth changes of R1 spin-labeled residues of the MPER upon 2F5 binding. Depth values of MPER R1 residues in the absence and the presence of 2F5 binding are indicated with blue and magenta bars, respectively. Depth values between -5 Å and 0 Å and greater than 0 Å correspond to lipid head group region and acyl chain region, respectively. The precise immersion depths of residues exposed to aqueous phase (depth < -5 Å) cannot be determined experimentally and are thus indicated by the striped bars. The biggest immersion depth changes are boxed in the light blue area. (*D*) Immersion depth of R1 residues of the MPER in the absence (purple columns) and the presence (yellow columns) of Z13e1.

To first examine the changes in MPER orientation induced by 2F5, membrane immersion depth values of spin-labeled residues in MPER peptide upon mAb binding were compared to that of MPER alone (Fig. 1*C*). Four spin-labeled residues (L669, W670, W672, and F673) located C-terminally to the 2F5 epitope in the MPER N helix and not exposed to solvent were chosen to provide meaningful measurements without abolishing 2F5 binding. Remarkable immersion depth changes were observed with L669R1 and W670R1 upon 2F5 binding (Fig. 1*C*). L669R1, deeply buried in the acyl chain region of lipid bilayer (depth >8 Å) before mAb binding, was lifted out of the membrane surface by 2F5 and exposed to the aqueous phase. W670R1 was moved into the lipid head group region, whereas the W672R1 and F673R1 residues were raised slightly up but remained in the acyl chain region. Little changes were observed with residues analyzed in the MPER C helix. Given these results and those from crystal structures of 2F5 in the complex with peptides (19–21), the 2F5-bound MPER segment likely encompasses an N-terminal extended "EL" region, followed by a type I β-turn motif at the core "DKW" epitope leading to W670 in a helical configuration connected to the MPER hinge and the C helix (Fig. 2*D*). Hence, as predicted by the 2-step conformational change model by BIAcore shared in common with 4E10 (ref. 22 and references therein), 2F5 may first interact with surface-exposed residues (E662 to D664), followed by extraction of buried residues (K665 and W666) into its binding pocket, subsequently lifting up the entire MPER N helix. Of note, the nonneutralizing but 2F5-crossblocking mAb 13H11 (22) failed to react with the membrane-embedded MPER by BIAcore (Fig. S4). The 13H11 epitope in the MPER includes L669 in the sequence "DKWASLW," and mutation of L669 to alanine abrogates 13H11 binding to the MPER (B. F. Haynes, M. S. Alam, and G. D. Tomaras, personal communication). The fact that residue L669 is membrane-embedded (Fig. 1*B*) indicates a different configuration of the MPER on the membrane from that in the soluble recombinant immunogen–group M shortened consensus (CON-S) gp140 envelope oligomer used to elicit 13H11 (22). This finding emphasizes the importance of a membrane environment for the relevant native MPER configuration.

To define the orientation of the MPER in complex with a third BNAb, Z13e1, we generated spin-labeled mutant MPERs at each residue position from W666 to W680. The affinities of Z13e1 to each cysteine-substituted, spin-labeled MPER peptide by BIAcore analysis (Fig. S5) were consistent with previous competitive ELISA studies using alanine-substituted MPER peptides (11). Membrane depth values were then determined for spin-labeled MPER peptides that retained greater than 50% Z13e1-binding reactivity relative to control MPER. No extraction of buried MPER residues was observed upon Z13e1 binding (Fig. 1*D*). W672R1 and F673R1 at the hinge were only slightly lifted up within the acyl chain region of lipid bilayer. By contrast, W666R1 in the N helix and W678R1 and L679R1 in the C helix actually appear somewhat more immersed in the membrane, although similar effects of A667R1 and S668R1 may be accounted for in part by shielding at the Z13e1 interface. Overall, unlike 4E10 and 2F5, Z13e1 only subtly changed the MPER membrane orientation without extracting buried residues in hinge or helical segments.

Downloaded at Palestinian Territory, occupied on December 19, 2021
www.manaraa.com

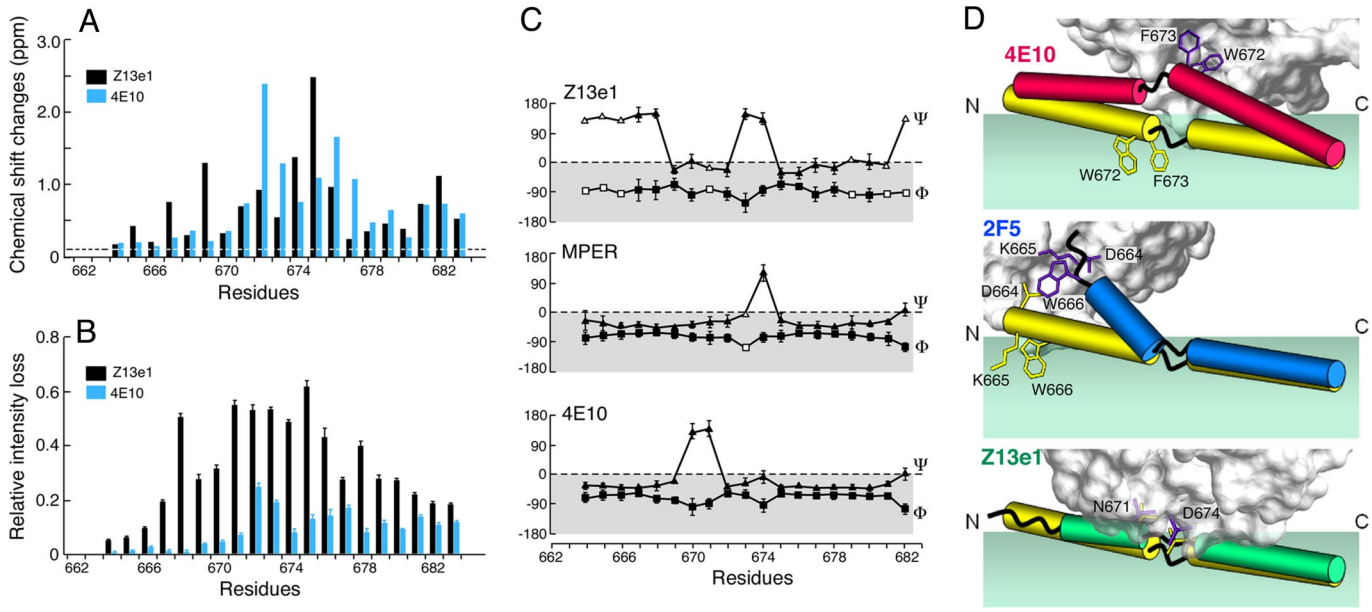

Fig. 2. Comparison of MPER conformational changes induced by Z13e1 and 4E10. (*A*) Normalized amide chemical shift changes {calculated as $[(\Delta Hcs)^2 + (\Delta Ncs/5)^2]^{1/2}$} of Z13e1 Fab-bound (black) and 4E10 Fab-bound (blue) MPERs relative to the unbound peptide in DPC micelles. Indicative chemical shift change (0.1 ppm) is shown with a dotted line. (*B*) MPER residues involved in Z13e1 (black) and 4E10 (blue) interactions shown by NMR cross-saturation transfer are indicated by relative signal reduction of amide peaks after 250-ms irradiation in methyl region. Cross-saturation transfer efficiencies are higher in Z13e1-bound MPERs because of higher immobility induced by tight Fab binding. The error bars represent statistical errors resulting from uncertainties in peak integration. (*C*) Comparison of backbone dihedral angles of the MPER in the absence (*Middle*) and presence of Z13e1 (*Top*) and 4E10 (*Bottom*), predicted from chemical shift values of Cα/Cβ. The Φ and Ψ angles are shown in square and triangle symbols, respectively (symbols in white correspond to statistically less reliable predictions). (*D*) Artistic rendering of MPER orientation changes induced by 4E10, 2F5, and Z13e1. Unbound MPER peptides (yellow tubes) are immersed in the lipid bilayers (light green panel). Red, blue, and green tubes represent the membrane orientation of schematic MPER segments in complex with 4E10, 2F5, and Z13e1 (gray surface area), respectively. N and C termini of MPER peptides are marked by letters N and C, respectively. Several key binding residues' positions are indicated before (yellow) and after (purple) antibody binding. For simplicity, the exact 3-dimensional features of MPER segments and Fabs are not visualized here. (See Fig. S9 for examples of structural details.)

MPER Conformational Changes upon Z13e1 Binding Revealed by NMR. To further characterize any Z13e1-induced MPER conformational changes, we obtained NMR spectra of Z13e1 Fab-bound MPER peptide ($^2H^{13}C^{15}N$-isotopically labeled) in the presence of dodecylphosphocholine (DPC) micelles. Three clusters, including residues A667 and L669, residues N671 to T676, and residues Y681 to K683, show large (>0.5 ppm) chemical shift changes (Fig. 2*A*). The 2 most affected residues are D674 and I675, in agreement with D674 being the key epitope residue for Z13e1 binding. Compared with the chemical shift change pattern found for 4E10 binding (of the wild-type MPER), the Z13e1-binding site extends more toward the N terminus (Fig. 2*A*). Because chemical shift change can be induced by both direct binding and indirect conformational change effects, we carried out NMR saturation transfer experiments to directly gauge the Z13e1-binding site on MPER. Fully deuterated MPER peptides in deuterated DPC micelles were mixed with the protonated Z13e1 Fab. By saturating methyl proton signals from the Z13e1 Fab, we observed magnetization cross-saturation transfers to the MPER amide groups that are in close contact with the antibody. As shown in Fig. 2*B*, the Z13e1 contacts amide groups extending from S668 to Y681. Distinct NOE peaks were observed in a ^{15}N-NOESY experiment between amide protons of residues including (but not limited to) A667, S668, F673, D674, N677, and Y681 to K683 from the MPER and aliphatic protons from Z13e1, indicating contacts with distances typically less than 5 Å (Fig. S6). These results suggest that Z13e1 contacts residues across the central MPER hinge region, like 4E10; however, it has a more extended binding site along the MPER compared with that of 4E10.

By using the $^2H,^{13}C,^{15}N$-isotopically labeled MPER bound to Z13e1 Fab, we determined the characteristic ^{13}C chemical shifts of their C′, Cα, and Cβ atoms of each residue (Fig. S7). Based on their secondary structure-induced systematic chemical shift changes, we used TALOS (23) software to predict the backbone dihedral angles of the Z13e1-bound MPER peptide. Several findings are noteworthy. First, after Z13e1 binding, the N-terminal residues of MPER up to S668 become extended or even unstructured (Fig. 2*C*). Second, the Z13e1-bound MPER otherwise retains nearly the same helical pattern, and perhaps overall conformation, at the antibody-binding site (Fig. 2*C Top* and *Middle*) as the unbound MPER, in contrast to the large conformational change induced by 4E10 binding (Fig. 2*C Middle* and *Bottom*). Third, the backbone Φ and Ψ predictions for the helical segments of Z13e1-bound MPER, from L669 to W672 and from I675 to Y681, deviate significantly from the typical α-helical values of −57° and −47° compared with micelle-bound MPER in the absence of Z13e1, which has more regular helical dihedral angles. These changes indicate that Z13e1 probably distorts slightly the local conformations of each residue while largely maintaining the overall peptide conformation (Fig. 2*D*). This is consistent with the fact that Z13e1 does not interact with the model viral membrane in our assays (17), instead binding to only those exposed or partially exposed MPER residues accessible on the membrane surface.

Z13e1 Immobilizes the MPER. The NMR spectra of saturation transfer experiments show that the Z13e1-bound MPER residues have more than twice the cross-saturation transfer efficiency compared with 4E10-bound peptide in their overlapping binding area. Hence, Z13e1 binds the MPER segment itself more tightly than 4E10 and rigidifies the bound peptide. The mobility changes of the MPER peptide upon Z13e1 binding can be visualized by the dramatic decrease in the NMR peak intensity between residues S668 and L679 (Fig. 3*A*). The N-terminal residues up to W666 and the

MICROBIOLOGY

Downloaded at Palestinian Territory, occupied on December 19, 2021
www.manaraa.com

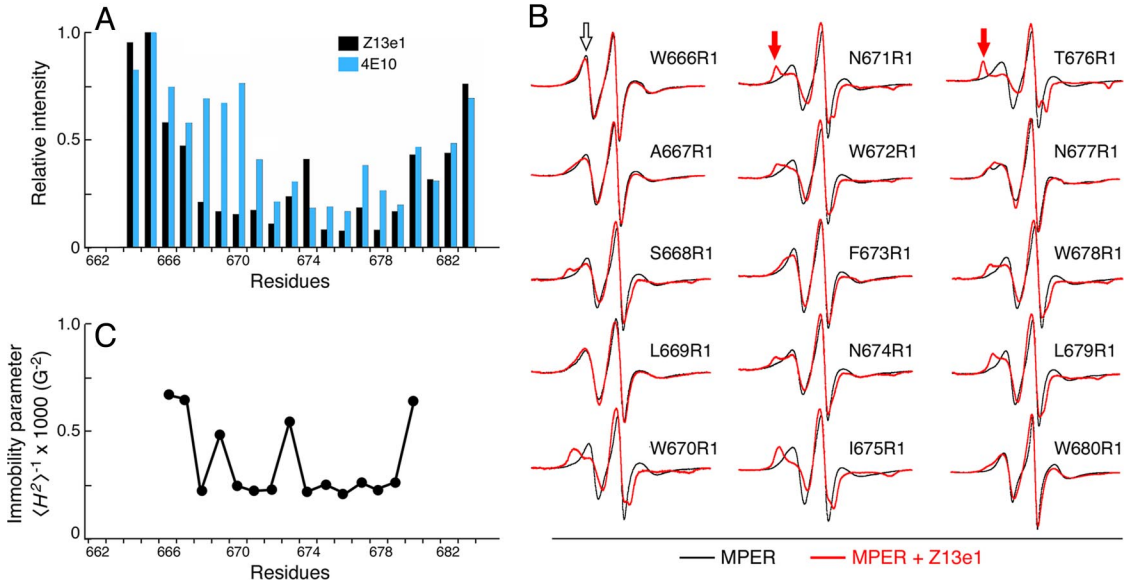

Fig. 3. MPER mobility changes upon Z13e1 binding by NMR and EPR. (*A*) Ratio of relative NMR intensities (using residue K665 as reference intensity) between Z13e1-bound and unbound MPER peptide (black) and between 4E10-bound and unbound MPER peptide (blue). Residues from S668 to L679 in Z13e1-bound MPER are highly immobile. In contrast, only residues from N671 to I682 in 4E10-bound MPER are highly immobile. (*B*) EPR spectra of R1 side chains in the MPER. Black traces indicate spectra obtained in the absence of Z13e1. Spectra recorded in the presence of 2-fold molar excess of Z13e1 to peptide are identified by the red traces. Features attributive to highly mobile spectra (W666R1) and highly immobile ones (N671R1 and T676R1) are marked by arrows in white and in red, respectively. All spectra were acquired at 2-mW incident microwave power with a 2-G modulation amplitude and a 100-G scan width. (*C*) Plot of immobility parameter (the inverse of second moment, $\langle H^2\rangle^{-1}$) of each of the EPR spectra with bound Z13e1 mAb. Large $\langle H^2\rangle^{-1}$ value corresponds to highly mobile residues.

C-terminal K683 are extremely mobile compared with the rest of the peptide, suggesting these residues are most likely unstructured. This is in contrast to 4E10-bound MPER as described in our prior analysis, where the N-terminal helical segment (shortened from the C-terminal end by 3 residues) is largely mobile as a single structural unit (17).

Consistent with the NMR findings, pronounced EPR spectral changes were observed for residues at or near the proposed epitope (11) upon Z13e1 binding. For residues S668R1, W670R1, N671R1, W672R1, N674R1, I675R1, T676R1, W678R1, and L679R1, spectra with broader peak-to-peak splitting were found compared with mAb-free MPER side chains, indicating decreased mobility of these R1 residues (Fig. 3*B*). The broadening of the EPR spectra of Z13e1-bound MPER peptides was quantified by reciprocal second-moment determination of the line shapes of each EPR spectra (Fig. 3*C*). Fig. 3*C* shows that the interaction region of MPER segments and Z13e1 most likely includes residues S668 to L679. Notably, deeply buried L669R1 and F673R1 are relatively flexible compared with their neighboring residues, suggesting that those 2 side chains are less motion-restricted and probably extend away from the mAb interface. Therefore, Z13e1 recognizes the aqueous phase-facing surface of the MPER. The initial interaction with pivotal residues N671 and D674 for Z13e1 binding (11) may subsequently establish close backbone and side-chain contacts with a large number of MPER residues encompassing both the N and C helices of MPER. The Z13e1-bound MPER is immobilized in the segment from S668 to L679 much more profoundly than the 4E10-bound MPER (Fig. 3*A*). With a relatively larger number of MPER residues in the binding site, possibly including main-chain interactions, Z13e1 achieves tighter binding without the deep binding pockets found in 4E10 and 2F5. By clamping down on its epitope residues, Z13e1 freezes any MPER hinge mobility, permitting only limited conformational changes at the membrane interface (Fig. 2*D*).

Important Contribution of W680 to 4E10 Binding and Membrane Reorientation of the MPER. Although the linear epitope sequences of 4E10 and Z13e1 binding coincide in the central MPER region, 4E10 involves residues that extend more C-terminally (Fig. 1*A*). Among surface-exposed residues, N671 and W680 are probably initial contact residues between 4E10 and the membrane-embedded MPER (Fig. 4*A*) (17), with N671 also crucial for Z13e1 but W680 unique for 4E10. We therefore asked whether primary contact of W680 by 4E10 may contribute to its subsequent epitope extraction and/or membrane MPER reorientation after membrane interaction, as described previously (17).

To experimentally examine the role of W680 in 4E10 function, membrane immersion depths of L669R1 and W678R1 were measured as references for 4E10-induced MPER conformational change. As shown in Fig. 4*B*, the binding reactivity of 4E10 to both L669R1/W680A and W678R1/W680A mutant MPER was slightly reduced but comparable to that of 4E10 binding to control MPER by BIAcore. However, the mobility change of L669R1/W680A and W678R1/W680A MPER mutants upon 4E10 binding was diminished compared with wild-type MPER, as shown by the EPR spectra in Fig. 4*C*, indicating that the W680A mutant affects 4E10 interaction with MPER. Perhaps more importantly, no immersion depth change of L669R1 in the W680A MPER variant was observed upon 4E10 binding, whereas it was evident that L669R1 was lifted from the membrane acyl chain region to the lipid head group region for the wild-type MPER (Fig. 4*D*). Note that the W678R1 in the W680A MPER variant remains in the acyl group region, similarly to that in wild-type MPER upon 4E10 binding. In contrast, the membrane depth change of the L669R1 residue was detected with N677A mutant MPER, although somewhat less compared with wild-type MPER (Fig. S8). Of note, surface-exposed N677 is involved in contact with both Z13e1 and 4E10. These data suggest that the initial interaction of W680 with the 4E10 CDRH3 loop allows the MPER to wrap around the base of the membrane-anchored 4E10 and bring the key epitope residues in the central hinge region closer to the hydrophobic 4E10 CDRH2 loop for extraction (Fig. S9).

Discussion

All 3 BNAbs inhibit MPER hinge motion, either by perturbing MPER membrane orientation of the N helix (2F5) or extraction of

Downloaded at Palestinian Territory, occupied on December 19, 2021
www.manaraa.com

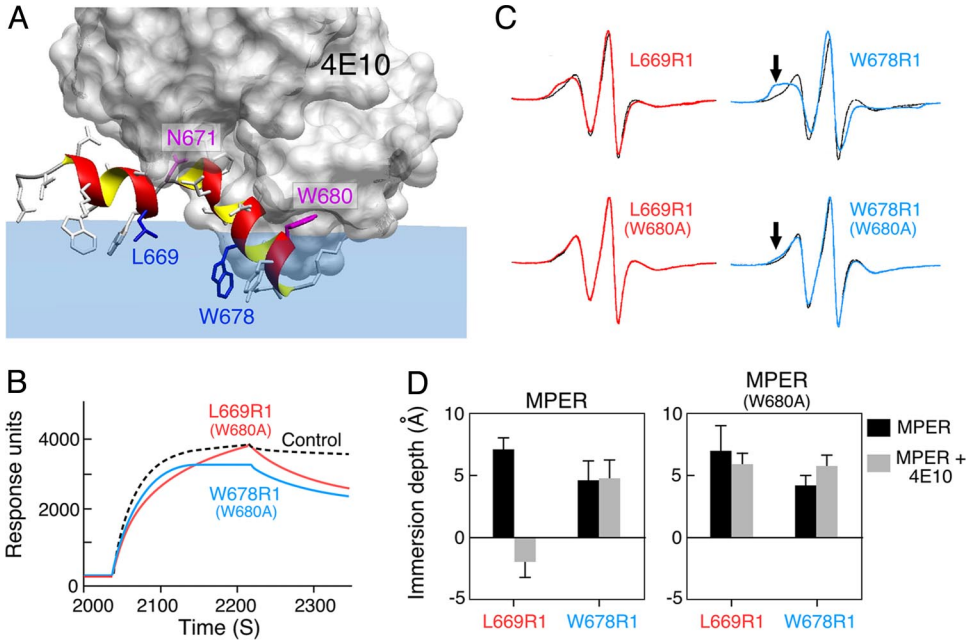

Fig. 4. Important contribution of W680 to the 4E10-induced MPER reorientation. (*A*) Model of MPER segment in complex with 4E10 antibody as viewed from the side. Residues proposed to be involved in 4E10 initial contact (N671 and W680) are in magenta, and reference residues for immersion depth changes are indicated in blue. Of note, the alanine mutations of initial contact residue N671 or core epitope residues W672 and F673 individually abolish 4E10 binding to the membrane-bound MPER by BIAcore analysis (17). (*B*) BIAcore sensograms of 4E10 binding to MPER variants on liposomes. 4E10 binding to spin-labeled peptides, L669R1/W680A and W678R1/W680A, is compared with that of 4E10 to unlabeled control MPER (HxB2). (*C*) 4E10-induced EPR spectra changes of spin-labeled side chains with and without W680A mutation. Black and colored traces indicate the spectra in the absence and the presence of 4E10, respectively. The decreased immobility upon 4E10 binding in W680A mutants is indicated by arrows. (*D*) Immersion depth changes of L669R1 and W678R1 in the control MPER and W680A MPER variant are compared in the absence (black columns) and the presence (gray columns) of 4E10. Depth values corresponding to different membrane regions are plotted as described in Fig. 1.

the centrally disposed MPER hinge (4E10) or by rigidifying the MPER segment over an extended surface contact area (Z13e1). The hinge confers independent movement of C and N helical segments of the MPER (and more N-terminal elements of gp41), facilitating structural rearrangement at reduced energetic cost during the fusion process. The apparent plasticity of the N helix segment upon antibody binding, as observed with all 3 BNAbs (Fig. 2*D*), underscores a more metastable segment N-terminal to the central hinge MPER region and is noteworthy for harboring the 3 tryptophan residues critical for membrane fusion (16). Conversely, the persistent configuration of the MPER C helix argues that this may be the conserved native state configuration, a true "Achilles' heel." 2F5 and 4E10 may exploit the naturally occurring motion and flexibility at the MPER N terminus and hinge to extract buried hydrophobic residues to achieve tight binding. Taken together, these BNAbs may interfere with viral fusion by inhibiting membrane disruption at an early stage and/or by blocking interaction between the MPER and the other region(s) of gp41 at a late stage (24–28).

Z13e1 and 4E10 recognize overlapping epitopes, with 4E10 manifesting broader cross-reactivity and stronger neutralization potency than Z13e1 (11). The more hydrophobic 4E10 interactions confer broader cross-reactivity than Z13e1, whose rigid binding to aqueous surface-exposed MPER elements can be inferred from biophysical parameters noted here and sequence-sensitive binding noted previously (11). Most of the 4E10 hydrophobic interactions occur in the deep binding pocket at the top or along one side of the MPER. We speculate that the latter interactions are largely missing from the Z13e1 interface but are compensated by the involvement of a greater number of MPER residues. Consequently, Z13e1 may be particularly vulnerable to structural rearrangement involving the N helix as a consequence of diminished affinity and/or stereohindrance. This difference may explain why, despite comparable binding affinities, 4E10 is ≈10-fold more potent at viral neutralization than Z13e1 (11).

Although it has been a difficult challenge to elicit BNAbs against MPER-related immunogens, the observation that such antibodies develop in a small fraction of HIV-positive individuals during infection offers optimism (29, 30). In that regard, our structural BNAb analysis sharpens the focus of immunogen design targeted to the MPER. For example, although theoretically any antibody ligating this segment with high affinity might confer neutralizing activity, conformational variability and frequent mutations in the most prevalent genetic subtype C may limit immunogen design targeting the 2F5-like epitope (31). Given minimal membrane contribution to binding involving multiple solvent-exposed residues, a protein scaffold immunogen approach seems warranted in an attempt to elicit Z13e1-like antibodies. However, sequence variability and key surface-exposed residues critical to this type of BNAb binding must be taken into design consideration. In that regard, 4E10-type antibodies are most advantageous, given sequence conservation of the C-terminal MPER segment and resulting neutralization breadth and potency. Elicitation of 4E10-like antibodies will likely require an MPER immunogen placed in a membrane context to induce both antibody interaction with the membrane and a capacity to extract conserved critical residues.

Materials and Methods

EPR. EPR spectroscopy was performed on a Bruker EMX spectromenter as described previously (17), with minor modifications. EPR spectra were recorded at 2-mW incident microwave power with a field modulation of 2.0 G at 100 kHz by using a Bruker high-sensitivity resonator. Power saturation measurements were carried out with microwave power varying from 0.4 to 100 mW and using a loop-gap resonator (JAGMAR) (17, 32, 33). Samples were placed in gas-permeable TPX tubes (Molecular Specialties) and purged by either a stream of air or N_2 gas. There was 5 mM NiEDDA used for periodicity

Downloaded at Palestinian Territory, occupied on December 19, 2021
www.manaraa.com

measurements, and 25 and 50 mM NiEDDA were used for immersion depth determination. The immersion depth parameter, Φ, was calculated by the ratio of accessibility value Π of O_2 to NiEDDA. Depth standard curves were determined by using lipid vesicles containing trace amounts of spin-labeled lipids (1:500 by weight) in the presence and absence of 4E10 antibody. Spin labeling of synthesized peptides and surface plasmon resonance experiments are described in *SI Materials and Methods*.

NMR Experiments. For Z13e1-binding experiments, 0.56 mg of $^{15}N^{13}C^{2}H$-labeled MPER peptides (molecular mass, 3.2 kDa; final concentration, 0.64 mM) was mixed with approximately 0.67 mM Z13e1 Fab and 100 mM d38-DPC in 270 μL of 10 mM $NaPO_4$ buffer, pH 6.8. Backbone assignment data were acquired by using a Bruker Avance 750-MHz spectrometer, and cross-saturation experiments were run on a Varian Inova 600-MHz spectrometer. NMR data on 4E10-bound MPERs were extracted from a previous study (17). The parameters used for the cross-saturation experiment were identical to that study. The backbone dihedral angles were predicted based on the assigned Cα/Cβ chemical shift values by using the software TALOS (23).

Preparation of Fab Z13e1 from IgG. IgG Z13e1 was buffer-exchanged from PBS into 25 mM Tris·Cl and 1 mM EDTA, pH 8.5, and concentrated to 15 mg/mL by using Amicon ultracentrifugal filter devices (Millipore). Endoproteinase Lys-C (0.002 mg/mL; Sigma–Aldrich) was added to the antibody solution, and the mixture incubated for 4 h at 37 °C. The Lys-C cleavage activity was stopped by addition of 1 mM N-α-tosyl-L-lysyl-chloromethyl ketone (Sigma–Aldrich) and 400 mM leupeptin (Sigma–Aldrich). The digestion buffer was exchanged with PBS, as above, and the digested antibody mixture was depleted of undigested IgG and Fc fragment by 2 consecutive incubations with 1 mL (1 mg) of protein A-conjugated Sepharose beads (GE Healthcare) for 1 h at room temperature under gentle agitation. The Fab Z13e1-containing supernatant was collected and sterile-filtered (0.22 μm). Fab Z13e1 was verified by ELISA for reactivity against recombinant gp41 and was found to be greater than 95% pure by SDS/PAGE.

Preparation of Liposomes. Large unilamellar vesicles (LUVs) were prepared as described previously (34, 35). Lipids were mixed in chloroform and dried as thin films under a nitrogen gas stream. To remove residual organic solvent, the lipid films were further dried by vacuum pump for $\approx$16 h. The lipids were resuspended in 20 mM Hepes and 150 mM KCl, pH 7.0, and subjected to 10–15 freeze–thaw cycles, followed by extrusion 15 times through 2 sheets of polycarbonate membrane with a pore size of 100 nm (Avanti Polar Lipids). The concentrations of prepared LUVs were determined by phosphate contents as described previously (36). Vesicles with virion membrane mimic were prepared at the molar ratio 9:18:20:9:45 of dioleoyl phosphatidylcholine/sphingomyelin/dioleoyl phosphatidylethanolamine/dioleoyl phosphatidylglycerol/cholesterol. 1-Palmitoyl-2-oleoyl phosphatidylcholine/1-palmitoyl-2-oleoyl phosphatidylglycerol LUVs at a 4:1 molar ratio were used for power saturation measurements with MPER variants in the presence of 4E10 antibody for comparison with previously determined results (17).

ACKNOWLEDGMENTS. We thank Drs. Barton Haynes (Duke University Human Vaccine Institute) and Munir S. Alam (Duke University Human Vaccine Institute) for providing 13H11 mAb and SP62 peptide, and Kyoung Joon Oh and Piotr G. Fajer for helpful discussions. This work was supported by National Institutes of Health Grants AI43649 (to E.L.R. and G.W.) and AI69993 (to M.B.Z.), as well as Austrian Science Fund Grant J2845-B13 (to J.S.G.).

1. Feng Y, Broder CC, Kennedy PE, Berger EA (1996) HIV-1 entry cofactor: Functional cDNA cloning of a seven-transmembrane, G protein-coupled receptor. *Science* 272:872–877.
2. Harrison SC (2005) Mechanism of membrane fusion by viral envelope proteins. *Adv Virus Res* 64:231–261.
3. Chan DC, Fass D, Berger JM, Kim PS (1997) Core structure of gp41 from the HIV envelope glycoprotein. *Cell* 89:263–273.
4. Haynes BF, Montefiori DC (2006) Aiming to induce broadly reactive neutralizing antibody responses with HIV-1 vaccine candidates. *Expert Rev Vaccines* 5:347–363.
5. Wei X, et al. (2003) Antibody neutralization and escape by HIV-1. *Nature* 422:307–312.
6. Wyatt R, et al. (1998) The antigenic structure of the HIV gp120 envelope glycoprotein. *Nature* 393:705–711.
7. Stiegler G, et al. (2001) A potent cross-clade neutralizing human monoclonal antibody against a novel epitope on gp41 of human immunodeficiency virus type 1. *AIDS Res Hum Retroviruses* 17:1757–1765.
8. Zwick MB, et al. (2001) Broadly neutralizing antibodies targeted to the membrane-proximal external region of human immunodeficiency virus type 1 glycoprotein gp41. *J Virol* 75:10892–10905.
9. Burton DR, et al. (1994) Efficient neutralization of primary isolates of HIV-1 by a recombinant human monoclonal antibody. *Science* 266:1024–1027.
10. Calarese DA, et al. (2003) Antibody domain exchange is an immunological solution to carbohydrate cluster recognition. *Science* 300:2065–2071.
11. Nelson JD, et al. (2007) An affinity-enhanced neutralizing antibody against the membrane-proximal external region of human immunodeficiency virus type 1 gp41 recognizes an epitope between those of 2F5 and 4E10. *J Virol* 81:4033–4043.
12. Conley AJ, et al. (1994) Neutralization of divergent human immunodeficiency virus type 1 variants and primary isolates by IAM-41–2F5, an anti-gp41 human monoclonal antibody. *Proc Natl Acad Sci USA* 91:3348–3352.
13. Muster T, et al. (1993) A conserved neutralizing epitope on gp41 of human immunodeficiency virus type 1. *J Virol* 67:6642–6647.
14. Trkola A, et al. (1996) Human monoclonal antibody 2G12 defines a distinctive neutralization epitope on the gp120 glycoprotein of human immunodeficiency virus type 1. *J Virol* 70:1100–1108.
15. Suarez T, Nir S, Goni FM, Saez-Cirion A, Nieva JL (2000) The pre-transmembrane region of the human immunodeficiency virus type-1 glycoprotein: A novel fusogenic sequence. *FEBS Lett* 477:145–149.
16. Salzwedel K, West JT, Hunter E (1999) A conserved tryptophan-rich motif in the membrane-proximal region of the human immunodeficiency virus type 1 gp41 ectodomain is important for Env-mediated fusion and virus infectivity. *J Virol* 73:2469–2480.
17. Sun ZY, et al. (2008) HIV-1 broadly neutralizing antibody extracts its epitope from a kinked gp41 ectodomain region on the viral membrane. *Immunity* 28:52–63.
18. Altenbach C, Greenhalgh DA, Khorana HG, Hubbell WL (1994) A collision gradient method to determine the immersion depth of nitroxides in lipid bilayers: Application to spin-labeled mutants of bacteriorhodopsin. *Proc Natl Acad Sci USA* 91:1667–1671.
19. Julien JP, Bryson S, Nieva JL, Pai EF (2008) Structural details of HIV-1 recognition by the broadly neutralizing monoclonal antibody 2F5: Epitope conformation, antigen-recognition loop mobility, and anion-binding site. *J Mol Biol* 384:377–392.
20. Ofek G, et al. (2004) Structure and mechanistic analysis of the anti-human immunodeficiency virus type 1 antibody 2F5 in complex with its gp41 epitope. *J Virol* 78:10724–10737.
21. Barbato G, et al. (2003) Structural analysis of the epitope of the anti-HIV antibody 2F5 sheds light into its mechanism of neutralization and HIV fusion. *J Mol Biol* 330:1101–1115.
22. Alam SM, et al. (2008) Human immunodeficiency virus type 1 gp41 antibodies that mask membrane proximal region epitopes: Antibody binding kinetics, induction, and potential for regulation in acute infection. *J Virol* 82:115–125.
23. Cornilescu G, Delaglio F, Bax A (1999) Protein backbone angle restraints from searching a database for chemical shift and sequence homology. *J Biomol NMR* 13:289–302.
24. Noah E, Biron Z, Naider F, Arshava B, Anglister J (2008) The membrane proximal external region of the HIV-1 envelope glycoprotein gp41 contributes to the stabilization of the six-helix bundle formed with a matching N′ peptide. *Biochemistry* 47:6782–6792.
25. Munoz-Barroso I, Salzwedel K, Hunter E, Blumenthal R (1999) Role of the membrane-proximal domain in the initial stages of human immunodeficiency virus type 1 envelope glycoprotein-mediated membrane fusion. *J Virol* 73:6089–6092.
26. Frey G, et al. (2008) A fusion-intermediate state of HIV-1 gp41 targeted by broadly neutralizing antibodies. *Proc Natl Acad Sci USA* 105:3739–3744.
27. Huarte N, et al. (2008) The broadly neutralizing anti-human immunodeficiency virus type 1 4E10 monoclonal antibody is better adapted to membrane-bound epitope recognition and blocking than 2F5. *J Virol* 82:8986–8996.
28. Dimitrov AS, et al. (2007) Exposure of the membrane-proximal external region of HIV-1 gp41 in the course of HIV-1 envelope glycoprotein-mediated fusion. *Biochemistry* 46:1398–1401.
29. Binley JM, et al. (2008) Profiling the specificity of neutralizing antibodies in a large panel of plasmas from patients chronically infected with human immunodeficiency virus type 1 subtypes B and C. *J Virol* 82:11651–11668.
30. Li Y, et al. (2008) Analysis of the neutralization specificities in polyclonal sera derived from human immunodeficiency virus type-1 infected individuals. *J Virol* 83:1045–1059.
31. Bures R, et al. (2002) Regional clustering of shared neutralization determinants on primary isolates of clade C human immunodeficiency virus type 1 from South Africa. *J Virol* 76:2233–2244.
32. Farahbakhsh ZT, Altenbach C, Hubbell WL (1992) Spin labeled cysteines as sensors for protein-lipid interaction and conformation in rhodopsin. *Photochem Photobiol* 56:1019–1033.
33. Shin YK, Hubbell WL (1992) Determination of electrostatic potentials at biological interfaces using electron-electron double resonance. *Biophys J* 61:1443–1453.
34. Szoka F, et al. (1980) Preparation of unilamellar liposomes of intermediate size (0.1–0.2 mumol) by a combination of reverse phase evaporation and extrusion through polycarbonate membranes. *Biochim Biophys Acta* 601:559–571.
35. Hope MJ, Bally MB, Webb G, Cullis PR (1985) Production of large unilamellar vesicles by a rapid extrusion procedure. Characterization of size distribution, trapped volume and ability to maintain a membrane potential. *Biochim Biophys Acta* 812:55–65.
36. Böttcher CJF, van Gent CM, Pries C (1961) A rapid and sensitive sub-micro phosphorus determination. *Anal Chim Acta* 24:203–204.
37. Zhu P, et al. (2006) Distribution and three-dimensional structure of AIDS virus envelope spikes. *Nature* 441:847–852.
38. Zhu P, Winkler H, Chertova E, Taylor KA, Roux KH (2008) Cryoelectron tomography of HIV-1 envelope spikes: Further evidence for tripod-like legs. *PLoS Pathog* 4:e1000203.
39. Liu J, Bartesaghi A, Borgnia MJ, Sapiro G, Subramaniam S (2008) Molecular architecture of native HIV-1 gp120 trimers. *Nature* 455:109–113.
40. Zanetti G, Briggs JA, Grunewald K, Sattentau QJ, Fuller SD (2006) Cryo-electron tomographic structure of an immunodeficiency virus envelope complex in situ. *PLoS Pathog* 2:e83.

Downloaded at Palestinian Territory, occupied on December 19, 2021
www.manaraa.com